III. 研究成果の刊行に関する一

雑 誌

発表者氏名	論文タイトル	発表誌名	巻号	ページ	出版年
1	Funama Y, Nagasue N, Awai K, Sakamoto I, Kakei K, Shimamura M, Yamashita Y, Uetani M.	Radiation exposure of operator performing interventional procedures using a flat panel angiography system: evaluation with photoluminescence glass dosimeters	Jpn J Radiol.	28(6)	423-9	2010
2	Yamamoto K, Yamamoto H, Yoshida K, Kisanuki A, Hirano Y, Ohte N, Akasaka T, Takeuchi M, Nakatani S, Ohtani T, Sozu T	Prognostic factors for the progression of calcific aortic valve disease at the early and late stages in the Japanese - Japanese Aortic Stenosis Study (JASS) Retrospective Analysis- Hyperten Res	Hyperten Res	33(3)	269-74.	2010
3	Isogai T, Jinzaki M, Tanami Y, Kusuzaki H, Yamada M, Kuribayashi S.	Body weight-tailored contrast material injection protocol for 64-detector row computed tomography coronary angiography.	Jpn J Radiol.	29(1)	Aug-33	2010
4	Tanami Y, Ikeda E, Jinzaki M, Satoh K, Nishiwaki Y, Yamada M, Okada Y, Kuribayashi S.	Computed tomographic attenuation value of coronary atherosclerotic plaques with different tube voltage: an ex vivo study.	J Comput Assist Tomogr.	34(1)	58-63	2010
5	Konishi M, Sugiyama S, Sato Y, Oshima S, Sugamura K, Nozaki T, Ohba K, Matsubara J, Sumida H, Nagayoshi Y, Sakamoto K, Utsunomiya D, Awai K, Jinnouchi H, Matsuzawa Y, Yamashita Y, Asada Y, Kimura K, Umemura S	Pericardial fat inflammation correlates with coronary artery disease.	Atherosclerosis.	213(2)	649-55	2010
6	Shimizu K, Utsunomiya D, Nakaura T, Awai K, Oda S, Yanaga Y, Funama Y, Hirai T, Hashida M, Yamashita Y.	Uniform vascular enhancement of lower-extremity artery on CT angiography using test-injection monitoring at the central level of the scan range: a simulation flow phantom study with clinical correlation.	Acad Radiol.	17(9)	1153-7.	2010
7	Utsunomiya D, Oda S, Funama Y, Awai K, Nakaura T, Yanaga Y, Hirai T, Yamashita Y.	Comparison of standard- and low-tube voltage MDCT angiography in patients with peripheral arterial disease.	Eur Radiol.	20(11)	2758-65.	2010
8	Utsunomiya H, Yamamoto H, Kunita E, Kitagawa T, Ohashi N, Oka T, Yamazato R, Horiguchi J, Kihara Y.	Combined presence of aortic valve calcification and mitral annular calcification as a marker of the extent and vulnerable characteristics of coronary artery plaque assessed by 64-multidetector computed tomography	Atherosclerosis.	213(1)	166-72	2010
9	Ohashi N, Yamamoto H, Horiguchi J, Kitagawa T, Kunita E, Utsunomiya H, Oka T, Kohno N, Kihara Y.	Association between visceral adipose tissue area and coronary plaque morphology assessed by CT angiography.	JACC Cardiovasc Imaging.	3(9)	908-17.	2010
10	Horiguchi J, Yamamoto H, Arie R, Kiguchi M, Fujioka C, Ohtaki M, Kihara Y, Awai K.	Is It Possible to Predict Heart Rate and Range during Enhanced Cardiac CT Scan from Previous Non-enhanced Cardiac CT?	J Digit Imaging.	Sep 8. [Epub ahead of print]		2010
11	Kitagawa T, Yamamoto H, Horiguchi J, Ohashi N, Kunita E, Utsunomiya H, Kihara Y.	Effects of statin therapy on non-calcified coronary plaque assessed by 64-slice computed tomography.	Int J Cardiol	Jun 7. [Epub ahead of print]		2010
12	Teragawa H, Morita K, Shishido H, Otsuka N, Hirokawa Y, Chayama K, Tamaki N, Kihara Y.	Impaired myocardial blood flow reserve in subjects with metabolic syndrome analyzed using positron emission tomography and N-13 labeled ammonia.	Eur J Nucl Med Mol Imaging.	37(2)	368-76.	2010

No.	Authors	Title	Journal	Vol/Date	Pages	Year
13	Ueno K, Kawamura A, Onizuka T, Kawakami T, Nagatomo Y, Hayashida K, Yuasa S, Maekawa Y, Anzai T, Jinzaki M, Kuribayashi S, Ogawa S.	Effect of preoperative evaluation by multidetector computed tomography in percutaneous coronary interventions of chronic total occlusions.	Int J Cardiol.	Nov 23. [Epub ahead of print]		2010
14	Tanami Y, Ikeda E, Jinzaki M, Satoh K, Nishiwaki Y, Yamada M, Okada Y, Kuribayashi S.	Computed tomographic attenuation value of coronary atherosclerotic plaques with different tube voltage: an ex vivo study.	J Comput Assist Tomogr.	34(1)	58-63.	2010
15	Utsunomiya D, Fukunaga T, Oda S, Awai K, Nakaura T, Urata J, Yamashita Y.	Multidetector computed tomography evaluation of coronary plaque morphology in patients with stable angina.	Heart Vessels.	Dec 4. [Epub ahead of print]		2010
16	Funama Y, Nagasue N, Awai K, Sakamoto I, Kakei K, Shimamura M, Yamashita Y, Uetani M.	Radiation exposure of operator performing interventional procedures using a flat panel angiography system: evaluation with photoluminescence glass dosimeters.	Jpn J Radiol.	28(6)	423-9	2010
17	Shimizu K, Utsunomiya D, Nakaura T, Awai K, Oda S, Yanaga Y, Funama Y, Hirai T, Hashida M, Yamashita Y.	niform vascular enhancement of lower-extremity artery on CT angiography using test-injection monitoring at the central level of the scan range: a simulation flow phantom study with clinical correlation	Heart Vessels.	Dec 4. [Epub ahead of print]		2010
18	Yamada M, Jinzaki M, Imai Y, Yamazaki S, Imanishi N, Tanami Y, Yamazaki A, Aiso S, Kuribayashi S. Evaluation of severely calcified coronary artery	Evaluation of severely calcified coronary artery using fast-switching dual-kVp 64-slice computed tomography.	Circ J.	75(2)	472-3.	2011
19	Tanami Y, Jinzaki M, Yamada M, Imai Y, Segawa K, Kuribayashi S.	Improvement of in-stent lumen measurement accuracy with new High-Definition CT in a phantom model: comparison with conventional 64-detector row CT.	Int J Cardiovasc Imaging.	Jan 8. [Epub ahead of print]		2011
20	Utsunomiya H, Yamamoto H, Horiguchi J, Kunita E, Okada T, Yamazato R, Hidaka T, Kihara Y.	Underestimation of aortic valve area in calcified aortic valve disease: Effects of left ventricular outflow tract ellipticity.	Int J Cardiol	Jan 12. [Epub ahead of print]		2011
21	Horiguchi J, Fujioka C, Kiguchi M, Yamamoto H, Shen Y, Kihara Y.	In vitro measurement of CT density and estimation of stenosis related to coronary soft plaque at 100 kV and 120 kV on ECG-triggered scan.	Eur J Radiol.	77(2)	294-8.	2011
22	Matsumoto K, Jinzaki M, Tanami Y, Ueno A, Yamada M, Kuribayashi S.	Virtual monochromatic spectral imaging with fast kilovoltage switching: improved image quality as compared with that obtained with conventional 120-kVp CT.	Radiology.	259(1)	257-62.	2011
23	Okada T, Yamamoto H, Okimoto T, Otsuka K, Ishibashi K, Dohi Y, Fujii T, Tadehara F, Kurisu S, Hayashi Y, Kihara Y; Coronary Atherosclerosis Reduction Project (CARP)	Beneficial Effects of Valsartan on Target Lesion Revascularization After Percutaneous Coronary Interventions With Bare-Metal Stents.	Circ J.	2011 May 17.[Epub ahead of print]		2011
24	Oka T, Yamamoto H, Ohashi N, Kitagawa T, Kunita E, Utsunomiya H, Yamazato R, Urabe Y, Horiguchi J, Awai K, Kihara Y.	Association between epicardial adipose tissue volume and characteristics of non-calcified plaques assessed by coronary computed tomographic angiography.	Int J Cardiol	May 11. [Epub ahead of print]		2011
25	Yamamoto H, Ohashi N, Utsunomiya H, Kunita E, Ishibashi K, Horiguchi J, Kihara Y.	Coronary calcium score as a predictor for coronary artery disease and cardiac events in Japanese high-risk patients.	Circ J	in press		2011
	山本秀也	冠動脈石灰化スコア	循環器内科	68(6	613-618	2010
	山本秀也、北川知郎、木原康樹.	2. 特集：第74回日本循環器学会学術集会　粥状効果の退縮：その分子機構から臨床まで　冠動脈プラークに対するスタチン治療効果　—　MDCTによる	循環器専門医	18(2)	223-32.	2010
	山本秀也	MDCTでどこまでわかるか a. 冠動脈病変	Heart View	14(7)	744-752	2010
	山本秀也	カルシウムスコアの重要性	Rad Fan	9(3)	16-18.	2011

書籍

著者氏名	論文タイトル名	書籍全体の編集者名	書 籍 名	出版社名	出版地	出版年	ページ
		木原康樹、栗林幸夫	CT冠動脈造影実践学	中外医学社	東京	2010	
山本秀也	4.冠動脈プラークの評価と臨床応用2) スタチンによるプラーク性状の変化	小室一成、栗林幸夫	心CT05	文光堂	東京	2010	p55-61
山本秀也、木原康樹	「動脈硬化の内科治療に迫る―薬物治療とインターベンション―III 冠動脈疾患 1．冠動脈疾患を診断する―狭窄からプラーク性状の評価へ― 6） MDCT	伊藤浩	新心臓病プラクティス.	文光堂	東京	2010	113-118
山本秀也、木原康樹	「動脈硬化の内科治療に迫る―薬物治療とインターベンション―III 冠動脈疾患 1．冠動脈疾患を診断する―狭窄からプラーク性状の評価へ― 6） MDCT	佐田政隆、下村伊一郎、野出孝一、綿田弘孝編集	Annual Book 「血管糖尿病2001」	フジメディカル出版	東京	2011	101-106

ELSEVIER

Combined presence of aortic valve calcification and mitral annular calcification as a marker of the extent and vulnerable characteristics of coronary artery plaque assessed by 64-multidetector computed tomography

Hiroto Utsunomiya[a], Hideya Yamamoto[a,*], Eiji Kunita[a], Toshiro Kitagawa[a], Norihiko Ohashi[a], Toshiharu Oka[a], Ryo Yamazato[a], Jun Horiguchi[b], Yasuki Kihara[a]

[a] Department of Cardiovascular Medicine, Hiroshima University Graduate School of Biomedical Sciences, 1-2-3 Kasumi, Minami-ku, Hiroshima 734-8551, Japan
[b] Department of Clinical Radiology, Hiroshima University Graduate School of Biomedical Sciences, Hiroshima, Japan

ABSTRACT

Objective: We examined the association of aortic valve calcification (AVC) and mitral annular calcification (MAC) to coronary atherosclerosis using 64-multidetector computed tomography (MDCT).
Background: Valvular calcification is considered a manifestation of atherosclerosis. The impact of multiple heart valve calcium deposits on the distribution and characteristics of coronary plaque is unknown.
Methods: We evaluated 322 patients referred for 64-MDCT, and assessed valvular calcification and the extent of calcified (CAP), mixed (MCAP), and noncalcified coronary atherosclerotic plaque (NCAP) in accordance with the 17-coronary segments model. We assessed the vulnerable characteristics of coronary plaque with positive remodeling, low-density plaque (CT density ≤38 Hounsfield units), and the presence of adjacent spotty calcification.
Results: In 49 patients with both AVC and MAC, the segment numbers of CAP and MCAP were larger than in those with a lack of valvular calcification and an isolated AVC (p < 0.001 for both). Multivariate analyses revealed that a combined presence of AVC and MAC was independently associated with the presence (odds ratio [OR] 9.36, 95% confidence interval [95%CI] 1.55–56.53, p = 0.015) and extent (β-estimate 1.86, p < 0.001) of overall coronary plaque. When stratified by plaque composition, it was associated with the extent of CAP (β-estimate 1.77, p < 0.001) and MCAP (β-estimate 1.04, p < 0.001), but not with NCAP. Moreover, it was also related to the presence of coronary plaque with all three vulnerable characteristics (OR 4.87, 95%CI 1.85–12.83, p = 0.001).
Conclusion: The combined presence of AVC and MAC is highly associated with the presence, extent, and vulnerable characteristics of coronary plaque identified by 64-MDCT.

© 2010 Elsevier Ireland Ltd. All rights reserved.

1. Introduction

Valvular calcification is generally considered a manifestation of atherosclerosis. Particularly, aortic valve calcification (AVC) and mitral annular calcification (MAC) were reported to be independently associated with both cardiovascular risk factors [1] and coronary artery calcification (CAC) [2,3]. Recent epidemiological studies have also demonstrated that the combined presence of

AVC and MAC is independent of and incremental to traditional risk assessment for the prediction of cardiovascular events, and is more strongly associated with cardiovascular mortality than is AVC or MAC alone [4].

Recent advances in contrast-enhanced data acquisition using multidetector computed tomography (MDCT) enabled the detection of calcified coronary atherosclerotic plaque (CAP), mixed coronary atherosclerotic plaque (MCAP), and noncalcified coronary atherosclerotic plaque (NCAP), which was in good agreement with intravascular ultrasound [5,6]. Furthermore, 64-MDCT characterizes coronary plaque in terms of vascular positive remodeling, lipid-rich plaque, and adjacent spotty calcium, which may relate to the fact that vulnerable plaque is prone to rupture with subsequent coronary events [7,8].

Although AVC and MAC are believed to be associated with overall coronary plaque burden using invasive coronary angiography or noncontrast-enhanced CT [2,9], the impact of multiple heart valve

---

calcium deposits on the distribution and vulnerable characteristics of coronary plaque is unknown. Thus, this study aimed to evaluate the value of the combined presence of AVC and MAC in predicting the extent and vulnerable characteristics of coronary plaque in patients with proven or suspected coronary artery disease (CAD).

2. Methods

2.1. Study population

Between August 2007 and December 2009, we enrolled 578 consecutive patients with proven or suspected CAD who were referred for 64-MDCT for the follow-up or diagnosis of CAD at our institution. Exclusion criteria included prior percutaneous coronary intervention (n = 92) or coronary artery bypass grafting (n = 90), irregular heart rhythm including chronic atrial fibrillation (n = 25), serum creatinine >1.5 mg/dl (n = 15), prior aortic or mitral valve surgery (n = 8), acute coronary syndrome (n = 8), hemodynamic instability (n = 3), and allergy to iodinated contrast agent (n = 2). We also excluded 13 patients due to poor image quality (n = 10) and declined consent (n = 3). As a result, 322 patients (207 men, 66 ± 11 years) were prospectively enrolled in this study. The study was approved by the Hiroshima University Hospital's ethical committee, and written informed consent was obtained from all patients.

2.2. Covariates and risk factor assessment

Overnight fasting blood samples were collected and the serum total cholesterol, low-density cholesterol, high-density cholesterol, triglyceride, and high-sensitivity C-reactive protein levels were measured. The creatinine clearance (Ccr) was measured by Modification of Diet in Renal Disease study equation. Hypertension was defined as systolic blood pressure >140 mm Hg, diastolic blood pressure >90 mm Hg, or current antihypertensive therapy. Diabetes mellitus was defined as a fasting plasma glucose >126 mg/dl or treatment with a hypoglycemic agent. Hyperlipidemia was defined as a fasting serum total cholesterol of >200 mg/dl or treatment with a lipid-lowering agent. Patients were considered current smokers if they had smoked at least one cigarette per day in the last year.

2.3. MDCT scan protocol

MDCT examinations were performed using a 64-MDCT scanner (LightSpeed VCT, GE Healthcare, Little Chalfont, Buckinghamshire, UK). Before MDCT angiography, a coronary and valve calcium scan was performed with a prospective ECG-triggered at 75% after the R-wave. The precise scan protocol of the retrospective ECG-gated MDCT angiography was previously described [5]. All patients with an initial heart rate ≥60 beats/min were given an oral β-blocker (metoprolol 40 mg) to achieve a target heart rate of 50–60 beats/min. Sublingual nitroglycerin was administrated just before scanning. A body-weight-adjusted volume (0.6–0.7 ml/kg) of iodine contrast (Iopamiron 370, Bayer Healthcare, Berlin, Germany) was administered into the antecubital vein over the course of 10 s, followed by 25 ml of saline solution injected at 5.0 ml/s. The CT reconstructed image data were transferred to an offline workstation (Advantage Workstation Ver. 4.2, GE Healthcare) for post-processing and subsequent image analysis.

2.4. CAC scoring

The total CAC score was calculated based on the Agatston method [10] with dedicated software (Smartscore, version 3.5, GE Healthcare).

2.5. Coronary plaque evaluation

All coronary segments >2 mm in diameter were assessed using thin-slice maximal intensity projections, multiplanar reconstructions, and cross-sectional images rendered perpendicular to the vessel center line of each coronary segment (0.75 mm thickness). The presence and extent of CAP, MCAP, and NCAP were determined for each subject and evaluated in accordance with the modified American Heart Association classification with 17-coronary segments [11].

CAP was defined as any structure with a CT density ≥130 HU that could be visualized separately from the contrast-enhanced coronary lumen, and that could be assigned to the coronary artery wall. MCAP was defined as the presence of CAP and NCAP, either because the calcium was embedded within noncalcified plaque or because they were adjacent to each other within a coronary segment. NCAP was defined as any clearly discernible structure >1 mm² that could be assigned to the coronary artery wall in at least two independent image planes, and that had a CT density <130 HU but greater than the surrounding pericardial tissue [12].

We then determined the minimum CT density, vascular remodeling index, and adjacent calcium morphology as previously described [5]. Briefly, the minimum CT density was decided as each plaque density by setting at least five regions of interest (each region area = 1 mm²) in each plaque area, and low-density plaque was defined as lesions with a CT density ≤38 HU. Following measurement of the cross-sectional vessel area at each plaque site and proximal reference site of the same coronary artery, we calculated the vascular remodeling index. Positive remodeling was defined as a remodeling index >1.05. The presence and morphology of calcium deposits in or adjacent to each plaque site were determined. Spotty calcium was defined as calcium burden length <3/2 of vessel diameter and width <2/3 of vessel diameter.

2.6. Valvular calcification assessment

The presence of AVC and MAC were qualitatively assessed from both noncontrast and multi-projection images reconstructed from contrast CT datasets. AVC was defined as a calcification lesion just inferior to the origin of the coronary arteries and located at the aortic leaflets, including the valvular point of attachment [3]. MAC was located at the junction between the left atrium and ventricle.

For the subgroup of patients with AVC or MAC, valvular calcification scores were measured with the same software used in CAC scoring. As in prior studies, calcification of the aortic wall immediately connected to calcification of the aortic valve cusps was included in the AVC [2].

2.7. Statistical analysis

Continuous data were presented as mean ± SD or median (interquartile range). Categorical variables were presented as numbers and percentages. The Kruskal–Wallis test or ANOVA was used for group comparisons of continuous variables, and post hoc testing was performed using the Tukey's test or the Steel–Dwass method for variables with and without normal distribution, respectively. Group comparisons of binary variables were performed using Fisher exact or χ² test. Multivariate analyses included valvular calcification and were adjusted for potential confounders based on previous reports: age, gender, Ccr, and the traditional risk factors of body mass index, hypertension, diabetes mellitus, hyperlipidemia, current smoking, and family history of premature CAD. Spearman's correlation coefficient was calculated to evaluate the association between the severity of valvular calcification and the extent of coronary atherosclerosis, where log-transformed AVC, MAC, and CAC scores were used. A probability value of p < 0.05 was considered

significant. All statistical analysis was performed using SPSS 13.0 (SPSS Inc, Chicago, IL).

3. Results

3.1. Patient characteristics

There were 201 subjects (62%) with AVC and 53 (17%) with MAC. Of 17 coronary artery segments, there was an average of 4.2 ± 3.4 segments with any plaque, 3.5 ± 3.3 with CAP, 1.3 ± 1.7 with MCAP, and 0.8 ± 1.2 with NCAP. Of 201 subjects with coronary plaque burden, 84 (26%) had coronary plaque with all three vulnerable characteristics (vascular positive remodeling, low CT density, and adjacent spotty calcification).

Clinical characteristics and CT findings stratified by the presence of valvular calcification are presented in Table 1. The population of isolated MAC was small ($n = 4$); therefore, we excluded this subgroup. Compared with patients with no valvular calcification, those with isolated AVC and those with the combined presence of AVC and MAC were older and had a higher prevalence of hypertension, diabetes mellitus, and hyperlipidemia. There were no significant differences among the three groups in serum lipid and C-reactive protein levels.

3.2. Valvular calcification and overall coronary plaque burden

In a univariate analyses, patients with the combined presence of AVC and MAC had an 11-fold increase odds of having any coronary plaque (odds ratio [OR] 11.16, 95% confidence interval [95%CI] 2.58–48.39, $p = 0.001$) and greater extent of overall coronary plaque

burden (β-estimate 2.34, $p < 0.001$) as compared to those with a lack of valvular calcification. After adjustment for age, gender, Ccr, and traditional risk factors, the combined presence of AVC and MAC remained an independent predictor for the presence (OR 9.36, 95%CI 1.55–56.53, $p = 0.015$) and extent (β-estimate 1.86, $p < 0.001$) of coronary plaque, as well as male gender, hypertension, and diabetes mellitus.

3.3. Valvular calcification and the prevalence and distribution of CAP, MCAP, and NCAP

Fig. 1 shows a representative case with the combined presence of AVC and MAC presenting MCAP with vulnerable characteristics. The prevalence and distribution of CAP and MCAP escalated in proportion with the presence of valvular calcification (all $p < 0.001$), whereas the prevalence of NCAP showed no significant difference among the three groups (Table 1). Fig. 2A shows the multivariate adjusted OR for the presence of CAP, MCAP, and NCAP across categories of valvular calcification.

Table 2 summarizes the associations of the combined presence of AVC and MAC to the presence and extent of CAP, MCAP, and NCAP. Multivariate analysis showed that the combined presence of AVC and MAC remained an independent predictor for the presence and extent of CAP (OR 6.21, 95%CI 1.67–23.05, $p = 0.006$; β-estimate 1.77, $p < 0.001$) and MCAP (OR 5.35, 95%CI 1.94–14.73, $p = 0.001$; β-estimate 1.04, $p < 0.001$), as well as male gender and hypertension. Meanwhile, no significant relationship was noted between valvular calcification and NCAP in either univariate or multivariate models.

Table 1
Clinical characteristics and CT findings stratified by the presence of valvular calcification.

Characteristics	None ($N = 118$)	Isolated AVC ($N = 151$)	Combined presence of AVC and MAC ($N = 49$)	p
Clinical data				
Age (years)	59 ± 10	$69 \pm 9^{*}$	$73 \pm 7^{*,\dagger}$	<0.001
Male, n (%)	69 (59)	93 (63)	38 (78)	0.067
Body mass index (kg/m^2)	25 ± 7	24 ± 3	24 ± 4	0.457
Ccr (ml/min)	71 ± 14	67 ± 15	$63 \pm 15^{*}$	0.011
Hypertension, n (%)	60 (51)	116 (77)*	39 (80)*	<0.001
Diabetes mellitus, n (%)	43 (36)	77 (51)*	32 (65)*,†	0.002
Hyperlipidemia, n (%)	48 (41)	88 (58)*	26 (53)*	0.016
Current smoker, n (%)	48 (41)	51 (34)	11 (22)	0.075
Family history of CAD, n (%)	13 (11)	20 (13)	9 (18)	0.442
Total cholesterol (mg/dl)	205 ± 45	202 ± 36	194 ± 34	0.252
Triglycerides (mg/dl)	130 (91–191)	124 (92–173)	119 (87–178)	0.801
HDL cholesterol (mg/dl)	60 ± 19	59 ± 18	62 ± 21	0.565
LDL cholesterol (mg/dl)	123 ± 36	119 ± 29	112 ± 27	0.102
High-sensitivity CRP (mg/l)	0.5 (0.3–1.0)	0.6 (0.3–1.4)	0.8 (0.3–2.1)	0.260
Lipid-lowering agents, n (%)	21 (18)	47 (31)*	18 (37)*	0.013
CT findings				
CAC score	6 (0–51)	152 (27–476)*	288 (102–1020)*,†	<0.001
Prevalence of CAP, n (%)	62 (53)	131 (87)*	47 (96)*,†	<0.001
Prevalence of MCAP, n (%)	44 (37)	93 (62)*	39 (80)*,†	<0.001
Prevalence of NCAP, n (%)	44 (37)	78 (52)	25 (51)	0.059
Extent of CAP (segments)	1.7 ± 2.4	$3.3 \pm 2.3^{*}$	$5.4 \pm 3.4^{*,\dagger}$	<0.001
Extent of MCAP (segments)	0.6 ± 0.9	$1.6 \pm 1.8^{*}$	$2.3 \pm 2.0^{*,\dagger}$	<0.001
Extent of NCAP (segments)	0.6 ± 0.9	$1.0 \pm 1.4^{*}$	0.9 ± 1.4	0.013
Positive remodeling, n (%)	36 (31)	96 (64)*	37 (76)*,†	<0.001
Low CT density, n (%)	45 (38)	82 (54)*	31 (63)*	<0.001
Spotty calcification, n (%)	37 (31)	74 (49)*	29 (59)*	0.001
All three vulnerable characteristics, n (%)	19 (16)	44 (29)*	21 (43)*,†	0.001

Values are mean ± SD, number (percentage), or median (interquartile range). AVC = aortic valve calcification; CAC = coronary artery calcification; CAD = coronary artery disease; CAP = calcified coronary atherosclerotic plaque; Ccr = creatinine clearance; CRP = C-reactive protein; CT = computed tomography; HDL = high-density lipoprotein; LDL = low-density lipoprotein; MAC = mitral annular calcification; MCAP = mixed coronary atherosclerotic plaque; NCAP = noncalcified coronary atherosclerotic plaque.
* $p < 0.05$ vs. none.
† $p < 0.05$ vs. isolated AVC.
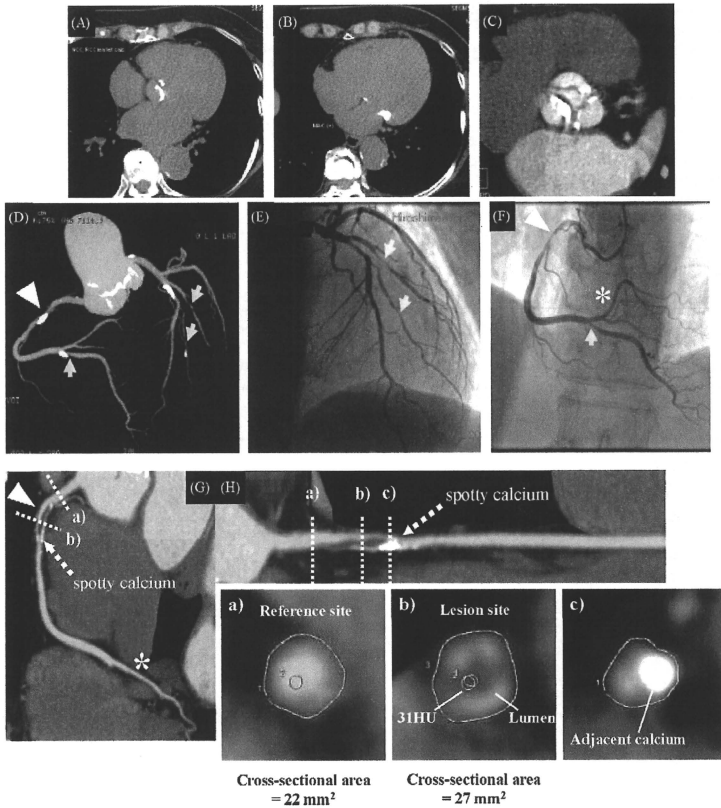
Fig. 1. A representative case with the combined presence of aortic valve calcification (AVC) (panel A) and mitral annular calcification (MAC) (panel B) presenting mixed coronary atherosclerotic plaque (MCAP) with vulnerable characteristics The double oblique transversal image shows calcified lesions at all leaflets (panel C). The maximum intensity projection image and invasive coronary angiography shows a severe stenosis of the proximal portion of the right coronary artery (arrowhead) and multiple obstructive lesions (panels D–F, yellow arrow). The multiplanar reconstruction image of the right coronary artery shows an obstructive MCAP with positive vascular remodeling and adjacent spotty calcium (panels G and H). The remodeling index is 1.23, calculated from the cross-sectional images of the reference site (a) and the lesion site (b). The minimum CT density of the lesion site is 31 HU. Adjacent spotty calcium can be observed in the cross-sectional image (c). (For interpretation of the references to colour in this figure legend, the reader is referred to the web version of the article.)

Table 2
Univariate and multivariate models for the associations of the combined presence of AVC and MAC to the presence and extent of CAP, MCAP, and NCAP.

	Presence		Extent	
	Odds ratio (95%CI)	p	β-estimate (95%CI)	p
CAP				
Univariate model	10.16 (3.44–30.06)	<0.001	2.27 (1.29–3.25)	<0.001
Multivariate model[a]	6.21 (1.67–23.05)	0.006	1.77 (0.83–2.72)	<0.001
MCAP				
Univariate model	6.56 (2.98–14.43)	<0.001	1.09 (0.60–1.59)	<0.001
Multivariate model[a]	5.35 (1.94–14.73)	0.001	1.04 (0.56–1.53)	<0.001
NCAP				
Univariate model	1.75 (0.89–3.43)	0.10	0.11 (−0.27–0.49)	0.56
Multivariate model[a]	1.45 (0.64–3.28)	0.37	−0.02 (−0.42–0.40)	0.97

CI = confidence interval. Other abbreviations as Table 1.

[a] Adjusted for age, gender, Ccr, and traditional risk factors including body mass index, hypertension, diabetes mellitus, hyperlipidemia, current smoking, and family history of coronary artery disease.
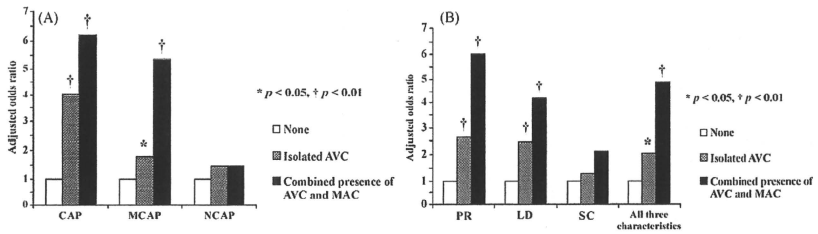
Fig. 2. Open bars represent no valvular calcification; hashed bars, isolated aortic valve calcification (AVC); solid bars, combined presence of AVC and mitral annular calcification (MAC). (A) Multivariate adjusted odds ratio for the presence of calcified coronary atherosclerotic plaque (CAP), mixed coronary atherosclerotic plaque (MCAP), and noncalcified coronary atherosclerotic plaque (NCAP) across categories of valvular calcification. (B) Multivariate adjusted odds ratio for the presence of coronary plaque with vulnerable characteristics (positive vascular remodeling [PR], low CT density [LD], adjacent spotty calcification [SC], and all three characteristics) across categories of valvular calcification.

3.4. Valvular calcification and coronary plaque with vulnerable characteristics

Patients with the combined presence of AVC and MAC had a higher frequency of coronary plaque with all three vulnerable characteristics than those with either no valvular calcification or isolated AVC (43% vs. 16% vs. 29%, respectively; $p = 0.001$). Fig. 2B depicts the multivariate adjusted OR for the presence of coronary plaque with vulnerable characteristics across categories of valvular calcification. Multivariate analysis showed that the combined presence of AVC and MAC remained an independent predictor for the presence of coronary plaque with all three vulnerable characteristics (OR 4.87, 95%CI 1.85–12.83, $p = 0.001$).

3.5. Valvular calcification score and the extent of coronary plaque

In a subgroup of patients with AVC ($n = 201$, 62%), the median AVC score was 77 (interquartile range 27–214). The AVC score correlated with the extent of coronary plaque, but its composition varied (Table 3). Multivariate analysis revealed that the log-transformed AVC score was not associated with the extent of CAP ($p = 0.07$), MCAP ($p = 0.19$), or NCAP ($p = 0.92$).

In a subgroup of patients with MAC ($n = 53$, 17%), the median MAC score was 82 (interquartile range 27–190). The MAC score did not correlate with the extent of coronary plaque ($p = 0.72$).

4. Discussion

Our study demonstrates the relationship between valvular calcification and the presence of coronary plaque with positive vascular remodeling, low CT density, and adjacent spotty calcium, which may represent vulnerable characteristics as previously reported [7,8]. These data suggest the presence of a common atherosclerotic pathway for development of valvular calcification and coronary

Table 3
Age- and gender-adjusted Spearman's correlation coefficients in patients with AVC ($n = 201$).

	Log(AVC + 1)	Log(CAC + 1)	CAP	MCAP	NCAP
Log(AVC + 1)	–				
Log(CAC + 1)	0.28[*]	–			
CAP	0.29[*]	0.88[*]	–		
MCAP	0.22[†]	0.53[*]	0.63[*]	–	
NCAP	−0.002	−0.12	−0.16[‡]	0.03	–

Abbreviations as Table 1.
[*] $p < 0.001$ for all correlations.
[†] $p < 0.01$ for all correlations.
[‡] $p < 0.05$ for all correlations.

plaque, and emphasize the importance of the combined presence of AVC and MAC as a marker of subclinical CAD.

4.1. Association between valvular calcification and coronary plaque burden

We demonstrate that valvular calcification is a marker of higher prevalence and severity of coronary plaque, particularly CAP and MCAP, independent of age and gender. The prevalence of AVC and MAC definitely increases with age [1], but is strongly related to traditional cardiovascular risk factors, including diabetes mellitus, hypertension [3], and hyperlipidemia [2]. Thus far, several studies have demonstrated a strong association of AVC or MAC with coronary microvascular endothelial dysfunction [13] and CAC, a marker of overall coronary atherosclerotic plaque burden [2,3]. Based on these data, it is believed that valvular calcification is a manifestation of atherosclerosis and is associated with CAD. However, paucity data exists regarding a direct association between the combined presence of AVC and MAC and the distribution of non-calcified plaque. Indeed, there is strong evidence that the severity of CAC is independent of and incremental to traditional risk factors for all-cause mortality and cardiovascular events [14]; whereas in a recent study, the number of segments with MCAP was an independent predictor of acute cardiac events [15]. Thus, our findings link the combined presence of AVC and MAC to the excess MCAP burden that leads to acute coronary events, and may assure early detection of MCAP for more accurate assessment of cardiovascular risk.

In this study, the combined presence of AVC and MAC was significantly associated with the presence and extent of MCAP, but not NCAP. Interestingly, Bamberg et al. recently demonstrated that the association between MCAP and NCAP was not constant but changed with age, indicating that the former is prominent in the early stages of atherosclerosis, whereas the latter develops during the chronic phase [16]. Therefore, our results suggest that the presence of multiple calcium deposits in heart valves could be a surrogate marker for the advanced stages of atherosclerosis. This observation is in agreement with a recent study that shows a significant relationship between AVC and the extent of coronary artery plaque [17].

4.2. Association between valvular calcification and coronary plaque vulnerability

Our study provides novel information on the age-independent association between valvular calcification and the vulnerable characteristics of coronary plaque. Several cohort studies have shown that patients with AVC [18] or MAC [19] had a higher risk of all-cause mortality and cardiovascular events, especially acute

coronary syndrome. In a recent report, the associations of AVC and MAC with cardiovascular mortality were strongest in patients with the combined presence of AVC and MAC [4]. Furthermore, an association between thoracic aortic calcification with total mortality was found in a prospective study with great number of subjects [20]. These data support the hypothesis that multiple calcium deposits in heart valves and thoracic aorta are a form of more advanced atherosclerosis with a high frequency of unstable coronary plaque, explaining its association with an increased risk of cardiovascular events.

A recent MDCT study demonstrated that noncalcified plaque is more strongly associated with the pathogenesis of acute coronary syndrome compared with CAP [7]. In addition, positive vascular remodeling, low CT density, and adjacent spotty calcium represent the coronary plaque vulnerability detected by 64-MDCT [8]. Considering our findings, we suggest that the combined presence of AVC and MAC may be used to improve risk stratification in clinical practice. Future prospective studies should evaluate whether the combined presence of AVC and MAC identifies patients at high risk for ischemic events, and whether medical treatment prevents these events.

4.3. Amounts of valvular calcification and subclinical coronary artery atherosclerosis

In this study, the severity of AVC was not independently associated with the extent of coronary plaque. In clinical practice, severe aortic stenosis caused by massive AVC with no obstructive CAD is often seen. These cases would be inapprehensible with a solely atherosclerotic mechanism of AVC progression. Recent noncontrast-enhanced CT studies have shown the two different phases of AVC progression: the early phase, when AVC appears *de novo* with progressive atherosclerosis, and the secondary phase, when established AVC progresses independently of cardiovascular risk factors and grows faster with calcification load [2]. Regarding MAC, echocardiographic severity has been directly related to the increased risk of cardiovascular events [19], whereas MAC severity was not correlated with the extent of coronary plaque in this study. Overall, our findings indicate that the combined presence of AVC and MAC is a marker of the presence and extent of coronary plaque, but massive valvular calcification is not a marker for extensive coronary plaque.

4.4. Limitations

This study was limited by a relatively small sample size. Our results cannot be generated because this is an observational and cross-sectional study. Thus, larger observational studies are necessary to confirm our findings. The study population was comprised of patients with proven or suspected CAD. A high prevalence of traditional risk factors and AVC were observed in this study. Thus, our results do not apply to patients with a lower probability of CAD. Furthermore, an additional mechanism related to renal insufficiency and osteoporosis may be responsible for the development of MAC. Because there were very few patients with isolated MAC in this study, the exact association between MAC and coronary plaque is not clear. However, the combined presence of AVC and MAC was shown to be incremental to isolated AVC in the prediction of coronary plaque with vulnerable characteristics.

Finally, cardiac MDCT examination should not be used for the sole purpose of AVC and MAC assessment due to its high radiation exposure. However, in this study, we performed 64-MDCT for the primary purpose of CAD assessment. The images obtained enabled evaluation of the association between valvular calcification and the extent and vulnerable characteristics of coronary atherosclerotic plaque.

5. Conclusions

Our study provides the first insight into the impact of the combined presence of AVC and MAC on the presence, extent, and vulnerable characteristics of coronary plaque in patients with proven or suspected CAD. The presence of multiple calcium deposits in heart valves is a useful marker for advanced coronary atherosclerosis, and is likely to help identify appropriate patients for aggressive medical therapy to inhibit the atherosclerosis process.

Conflict of interest

The authors declare no conflicts of interest.

Acknowledgements

References

[1] Stewart BF, Siscovick D, Lind BK, et al. Clinical factors associated with calcific aortic valve disease. Cardiovascular Health Study. J Am Coll Cardiol 1997;29:630–4.
[2] Messika-Zeitoun D, Bielak LF, Peyser PA, et al. Aortic valve calcification: determinants and progression in the population. Arterioscler Thromb Vasc Biol 2007;27:642–8.
[3] Allison MA, Cheung P, Criqui MH, Langer RD, Wright CM. Mitral and aortic annular calcification are highly associated with systemic calcified atherosclerosis. Circulation 2006;113:861–6.
[4] Volzke H, Haring R, Lorbeer R, et al. Heart valve sclerosis predicts all-cause and cardiovascular mortality. Atherosclerosis 2010;209:606–10.
[5] Kitagawa T, Yamamoto H, Ohhashi N, et al. Comprehensive evaluation of noncalcified coronary plaque characteristics detected using 64-slice computed tomography in patients with proven or suspected coronary artery disease. Am Heart J 2007;154:1191–8.
[6] Leber AW, Knez A, von Ziegler F, et al. Quantification of obstructive and nonobstructive coronary lesions by 64-slice computed tomography: a comparative study with quantitative coronary angiography and intravascular ultrasound. J Am Coll Cardiol 2005;46:147–54.
[7] Motoyama S, Sarai M, Harigaya H, et al. Computed tomographic angiography characteristics of atherosclerotic plaques subsequently resulting in acute coronary syndrome. J Am Coll Cardiol 2009;54:49–57.
[8] Kitagawa T, Yamamoto H, Horiguchi J, et al. Characterization of noncalcified coronary plaques and identification of culprit lesions in patients with acute coronary syndrome by 64-slice computed tomography. JACC Cardiovasc Imaging 2009;2:153–60.
[9] Yamamoto H, Shavelle D, Takasu J, et al. Valvular and thoracic aortic calcium as a marker of the extent and severity of angiographic coronary artery disease. Am Heart J 2003;146:153–9.
[10] Agatston AS, Janowitz WR, Hildner FJ, Zusmer NR, Viamonte Jr M, Detrano R. Quantification of coronary artery calcium using ultrafast computed tomography. J Am Coll Cardiol 1990;15:827–32.
[11] Raff GL, Abidov A, Achenbach S, et al. SCCT guidelines for the interpretation and reporting of coronary computed tomographic angiography. J Cardiovasc Comput Tomogr 2009;3:122–36.
[12] Hoffmann U, Bamberg F, Chae CU, et al. Coronary computed tomography angiography for early triage of patients with acute chest pain: the ROMICAT (Rule Out Myocardial Infarction using Computer Assisted Tomography) trial. J Am Coll Cardiol 2009;53:1642–50.
[13] Bozbas H, Pirat B, Yildirir A, et al. Mitral annular calcification associated with impaired coronary microvascular function. Atherosclerosis 2008;198:115–21.
[14] Budoff MJ, Shaw LJ, Liu ST, et al. Long-term prognosis associated with coronary calcification: observations from a registry of 25,253 patients. J Am Coll Cardiol 2007;49:1860–70.
[15] Pundziute G, Schuijf JD, Jukema JW, et al. Prognostic value of multislice computed tomography coronary angiography in patients with known or suspected coronary artery disease. J Am Coll Cardiol 2007;49:62–70.
[16] Bamberg F, Dannemann N, Shapiro MD, et al. Association between cardiovascular risk profiles and the presence and extent of different types of coronary atherosclerotic plaque as detected by multidetector computed tomography. Arterioscler Thromb Vasc Biol 2008;28:568–74.
[17] Mahabadi AA, Bamberg F, Toepker M, et al. Association of aortic valve calcification to the presence, extent, and composition of coronary artery

plaque burden: from the Rule Out Myocardial Infarction using Computer Assisted Tomography (ROMICAT) trial. Am Heart J 2009;158: 562–8.

[18] Otto CM, Lind BK, Kitzman DW, Gersh BJ, Siscovick DS. Association of aortic-valve sclerosis with cardiovascular mortality and morbidity in the elderly. N Engl J Med 1999;341:142–7.

[19] Kohsaka S, Jin Z, Rundek T, et al. Impact of mitral annular calcification on cardiovascular events in a multiethnic community: the Northern Manhattan Study. JACC Cardiovasc Imaging 2008;1:617–23.

[20] Santos RD, Rumberger JA, Budoff MJ, et al. Thoracic aorta calcification detected by electron beam tomography predicts all-cause mortality. Atherosclerosis 2010;209:131–5.
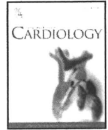
Underestimation of aortic valve area in calcified aortic valve disease: Effects of left ventricular outflow tract ellipticity

Hiroto Utsunomiya [a], Hideya Yamamoto [a,*], Jun Horiguchi [b], Eiji Kunita [a], Takenori Okada [a], Ryo Yamazato [a], Takayuki Hidaka [a], Yasuki Kihara [a]

[a] Department of Cardiovascular Medicine, Hiroshima University Graduate School of Biomedical Sciences, Hiroshima, Japan
[b] Department of Clinical Radiology, Hiroshima University Hospital, Hiroshima, Japan

ABSTRACT

Background: The aortic valve area (AVA) is usually calculated using the continuity equation (CE) in which the left ventricular outflow tract (LVOT) area is estimated assuming circular geometry. We sought to evaluate the LVOT ellipticity with 64-multidetector computed tomography (MDCT) and to assess the impact of LVOT ellipticity on the evaluation of CE-based AVA in patients with calcified aortic valves.
Methods: We prospectively studied 110 patients with calcified aortic valves including 54 aortic stenosis (AS) with both 64-MDCT and transthoracic echocardiography. Double oblique transversal images for planimetry of the aortic valve and LVOT were obtained during the midsystolic phase. The short and long-axis diameters of the planimetered LVOT were measured.
Results: The MDCT planimetered LVOT area was underestimated by the diameter-derived ($\pi \times r^2$) LVOT area using echocardiography (444 ± 70 mm^2 versus 369 ± 63 mm^2; p<0.001). The mean difference in AVA values calculated using the CE and planimetry was 0.43 ± 0.23 cm^2 and mean measurement error of CE-based AVA was 18%. When the CE-based AVA was corrected using the MDCT planimetered LVOT area, the measurement error decreased from 28 ± 5 to 5 ± 2% in patients with severe aortic stenosis (AVA < 1.0 cm^2), whereas from 16 ± 5 to 3 ± 6% in others.
Conclusion: Ellipticity of LVOT is associated with underestimation of AVA measurements using the CE. CE-based AVA corrected with MDCT planimetered LVOT area is useful especially in severe AS.

© 2010 Elsevier Ireland Ltd. All rights reserved.

1. Introduction

To assess the severity of aortic stenosis (AS) using Doppler echocardiography, aortic valve area (AVA) is usually estimated using the CE [1]: $AVA = LVOT\ area \times (VTI_{LVOT}/VTI_{AV})$, where $LVOT\ area$ is the cross-sectional area of the left ventricular outflow tract (LVOT) calculated from a measured LVOT diameter, with the assumption that the LVOT is circular. VTI is the velocity–time integral measured from Doppler tracings at the LVOT and aortic valve.

Although good correlation between planimetry and CE-based measurements of AVA has been obtained, planimetric AVA measurements always yield greater AVA values than those calculated using the CE [2]. Multidetector computed tomography (MDCT) can provide an accurate and noninvasive imaging technique, not only for the coronary artery, but also for aortic valve planimetry [3] and geometry including the aortic annulus and LVOT [4]. Several studies using 64-MDCT have demonstrated that the LVOT is elliptical rather than

round in shape [5,6]. It has also been found that the assumption of circular geometry in calculating the LVOT area using echocardiography and the CE ($\pi \times r^2$) consistently underestimates the actual LVOT area measured by MDCT in a wide variety of pathological conditions [5,6]. However, these investigations have not been sufficiently validated in patients with calcified aortic valve disease. Thus, we sought to extensively evaluate LVOT ellipticity with 64-MDCT and to assess the impact of LVOT ellipticity on the evaluation of AVA using echocardiography.

2. Methods

2.1. Study population

We prospectively recruited 163 consecutive patients referred for echocardiography and scheduled for subsequent MDCT angiography. Both examinations were performed within 1 week. Exclusion criteria included: grade > 2/4 aortic regurgitation; bicuspid aortic valve; previous surgery of the aortic valve or the ascending aorta; reduced LV contraction (LV ejection fraction <50%); and LVOT obstruction (LVOT flow velocity >2 m/s). A final number of 110 patients with aortic valve calcification were enrolled in the study. BMI was used as a marker of obesity: BMI (kg/m^2) = weight (kg)/height (m)^2. The body surface area (BSA) was calculated as follows: BSA (m^2) = $88.83 \times$ height (cm)$^{0.663} \times$ weight (kg)$^{0.444}$. The study protocol was approved for use by the Human Studies Subcommittee of Hiroshima University Graduate School of Biomedical Sciences. Prior written informed consent was obtained from all participants.

* Corresponding author. Department of Cardiovascular Medicine, Hiroshima University Graduate School of Biomedical Sciences, 1-2-3 Kasumi, Minami-ku, Hiroshima 734-8551, Japan. Tel.: +81 82 257 5540; fax: +81 82 257 1569.
E-mail address: hideyama@hiroshima-u.ac.jp (H. Yamamoto).
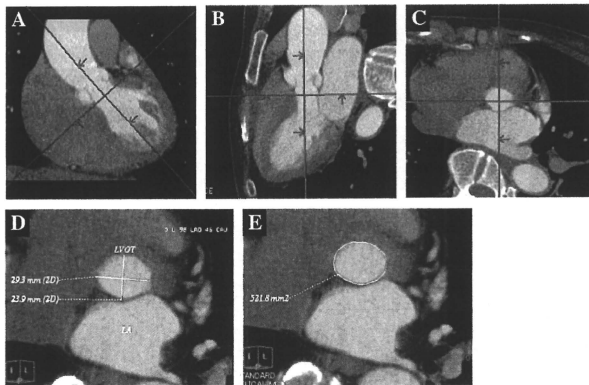
Fig. 1. The left coronal view (A) and the single oblique sagittal view (B) were reconstructed to measure the planimetric AVA. For the planimetry of the LVOT, the double oblique transversal view of the LVOT was reconstructed immediately below the aortic valve parallel to the plane used for measurement of the AVA (C). The short-axis image of the LVOT shows a clearly evident oval shape (D). The directly measured LVOT area is acquired by planimetry (E). AVA = aortic valve area; LVOT = left ventricular outflow tract; MDCT = multidetector computed tomography.

2.2. Multidetector computed tomography

The MDCT examinations were performed with a 64-MDCT scanner (LightSpeed VCT, GE Healthcare, Waukesha, WI). For the MDCT coronary angiogram, a collimation of 64×0.625 mm and a gantry rotation time of 350 ms were used. Standard scanning parameters were set to 120 kV and 600 mA. Following a test bolus examination to determine the start of the contrast-enhanced scan, a retrospective ECG-gated CT angiography was performed using a helical mode during an inspiratory breath-hold. The mean radiation dose for the group was 14.4 mSv. To avoid motion artifacts, all patients with an initial heart rate ≥60 beats/min were given an oral β-blocker (metoprolol 40 mg) to achieve a target heart rate of 50–60 bpm. A body weight-adjusted volume (0.6–0.7 mL/kg) of nonionic contrast material (Iopamiron 370, Bayer Healthcare, Berlin, Germany) was administrated via the antecubital vein over a period of 10 seconds, followed by 25 ml of saline solution injected at 5.0 mL/s. Image reconstruction was retrospectively gated to ECG. The dataset of the contrast-enhanced scan was reconstructed at every 5% of the R–R interval. Axial datasets were then transferred to a remote computer workstation (Advantage Workstation Ver.4.2, GE Healthcare) for post-processing and subsequent image analysis.

2.3. Image analysis

For the purpose of LVOT and aortic valve planimetry, we determined a plane perpendicular to the LVOT and aortic root using the double oblique method [3,4]. Namely, a left coronal and a single oblique sagittal view through the LVOT and aortic valve were reconstructed (Fig. 1A and B). Then, maximum effort was made to correctly orientate both planes by simultaneously reviewing the reconstructed double oblique transversal view of the aortic leaflet tips. Planimetry of the aortic valve was performed during the midsystolic phase, which provided the largest AVA with the fewest artifacts [7]. Likewise, planimetry of the LVOT cross-sectional area was performed just beneath the aortic annulus in a plane perpendicular to the LVOT long axis in the same phase as that used for the measurement of the AVA (Fig. 1C).

For the purpose of measurement of LVOT ellipticity, we measured the short- (a) and long- (b) axis diameters of the planimetered LVOT view. The ellipsoidal-estimated LVOT area was calculated using the equation for an ellipse ($\pi \times a/2 \times b/2$). Furthermore, the ellipticity index was calculated using the equation $1 - (a/b)$ to quantify the degree of deviation of the LVOT shape from a perfect circle (Fig. 1D and E). Using this index, an ellipticity index of zero represents a perfect circle with a higher index describing a more elliptical geometry.

Intra- and interobserver variability of MDCT measurements were calculated as the coefficient of variation in 10 randomly selected subjects. Intraobserver reproducibility was assessed for a single observer on two separate occasions and interobserver variability was performed by two independent experienced investigators.

2.4. Echocardiography

Comprehensive echocardiograms were performed by an experienced sonographer using high-quality commercially available ultrasound systems (GE Healthcare Vivid 7, Milwaukee, WI) equipped with S4 transducer. Images were obtained in the parasternal (long- and short axis) and apical views. LV volume and ejection fraction were calculated from apical 2- and 4-chamber views using the biplane Simpson's rule according to the recommendation of the American Society of Echocardiography [8]. LV mass was measured using M-mode echocardiography [9]. The LVOT diameter was measured during midsystole immediately below the aortic annulus from the parasternal long-axis view [8]. Using πr^2, the diameter-derived LVOT area was calculated. For the calculation of the CE-based AVA, VTI at the LVOT and the aortic

Table 1
Clinical characteristics, echocardiographic findings and MDCT measurements (n = 110).

Characteristics	Findings
Clinical data	
Age (years)	70 ± 9
Male (%)	47
Height (cm)	157 ± 10
Weight (kg)	58 ± 11
Body mass index (kg/m²)	23.5 ± 3.1
Body surface area (m²)	1.58 ± 0.19
Echocardiographic data	
Peak aortic valve velocity (m/s)	2.3 ± 1.3
CE-based AVA (cm²)	1.99 ± 0.84
Mild AS, n (%)	22 (20)
Moderate AS, n (%)	12 (11)
Severe AS, n (%)	20 (18)
LV end-diastolic volume (ml)	84 ± 24
LV end-systolic volume (ml)	26 ± 13
LV ejection fraction (%)	69 ± 9
Interventricular septal wall thickness (mm)	10.6 ± 2.0
LV posterior wall thickness (mm)	10.4 ± 1.6
LV mass index (g/m²)	101 ± 31
LVOT diameter (mm)	21.6 ± 1.8
MDCT measurements	
MDCT planimetered AVA (cm²)	2.47 ± 1.03
LVOT short axis diameter (mm)	21.3 ± 1.9
LVOT long-axis diameter (mm)	26.8 ± 2.4
Ellipsoidal-estimated LVOT area (mm²)	449 ± 72
MDCT planimetered LVOT area (mm²)	444 ± 70
Ellipticity index	0.20 ± 0.04

Values are expressed as mean ± SD or number (percentage).
AVA = aortic valve area; AS = aortic stenosis; CE = continuity equation; LVOT = left ventricular outflow tract; MDCT = multidetector computed tomography.

Table 2
Correlation of the MDCT planimetered LVOT area and the ellipticity index with demographic and echocardiographic variables.

Variables	LVOT area		Ellipticity index	
	Spearman's R	p	Spearman's R	p
Age	−0.34	<0.001	0.04	0.69
Height	0.63	<0.001	−0.17	0.07
Weight	0.51	<0.001	−0.08	0.39
Body surface area	0.57	<0.001	−0.13	0.17
Systolic blood pressure	0.09	0.63	−0.15	0.23
Peak aortic valve velocity	−0.13	0.19	0.39	<0.001
LV end-diastolic volume	0.41	<0.001	0.04	0.68
LV end-systolic volume	0.52	<0.001	0.01	0.91
Interventricular septal wall thickness	0.18	0.07	0.31	0.001
LV mass index	0.13	0.24	0.31	0.001
LVOT diameter	0.81	<0.001	−0.21	0.03

Abbreviations are as detailed in Table 1.

valve were recorded using pulse Doppler from the apical 5-chamber view. Peak aortic valve velocity and mean transaortic pressure gradient were measured in multiple views (apical long axis, apical 5-chamber and right parasternal) and the maximum values were used [10]. AS was defined as CE-based AVA<2.0 cm². Classification of AS was based on the recommendation of the American Society of Echocardiography (mild:

aortic valve restriction with AVA>1.5 cm², moderate: AVA 1.0 to 1.5 cm², and severe: AVA<1.0 cm²) [1].

2.5. Statistical analysis

All measurements were expressed as mean ± SD. The unpaired t test or Mann–Whitney U-test was used to compare continuous variables with or without normal distribution, respectively. The MDCT planimetered LVOT area was compared with the diameter-derived LVOT area and ellipsoidal-estimated LVOT area using a paired t test and Pearson's correlation coefficient r. Agreements between methods (MDCT planimetered LVOT area versus diameter-derived LVOT area; MDCT planimetered LVOT area versus ellipsoidal-estimated LVOT area; and CE-based AVA versus MDCT planimetered AVA) were tested using Bland–Altman analyses and plotted with lines representing the mean ± 2SD. Relationships between LVOT measurements and patients' demographic parameters were assessed using Spearman rank correlations. A probability value of p<0.05 was considered significant. All statistical analyses were performed using SPSS 12.0 (SPSS Inc, Chicago, IL).

3. Results

3.1. Relationships between LVOT measurements and demographic variables

Table 1 shows the clinical characteristics, echocardiographic findings and CT measurements of the study population. The mean CE-based
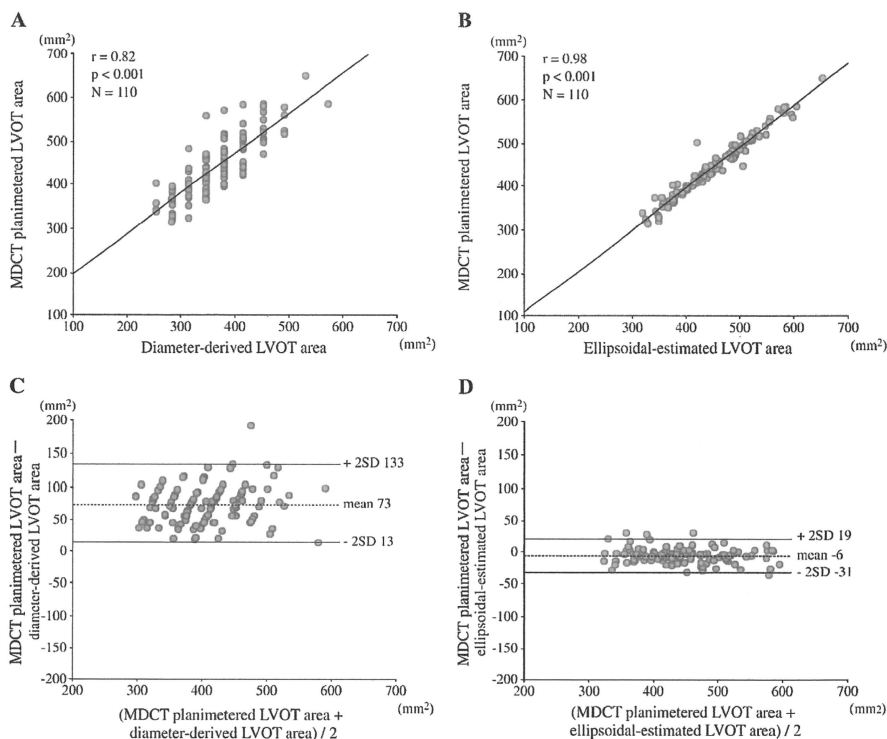
Fig. 2. Scatterplot of correlation between MDCT planimetered LVOT area and diameter-derived LVOT area calculated using echocardiography (A) and that between the MDCT planimetered LVOT area and the ellipsoidal-estimated LVOT area (B). Bland–Altman plot analysis shows that the MDCT planimetered LVOT area has a poor agreement with the diameter-derived LVOT area (C), whereas has a good agreement with the ellipsoidal-estimated LVOT area (D). Abbreviations are as detailed in Fig. 1.

AVA value was 1.99 ± 0.84 cm^2, including 54 patients with AS (mild, n=22; moderate, n=12; severe, n=20). Diameters of the ascending aorta measured by MDCT ranged from 30 to 44 mm.
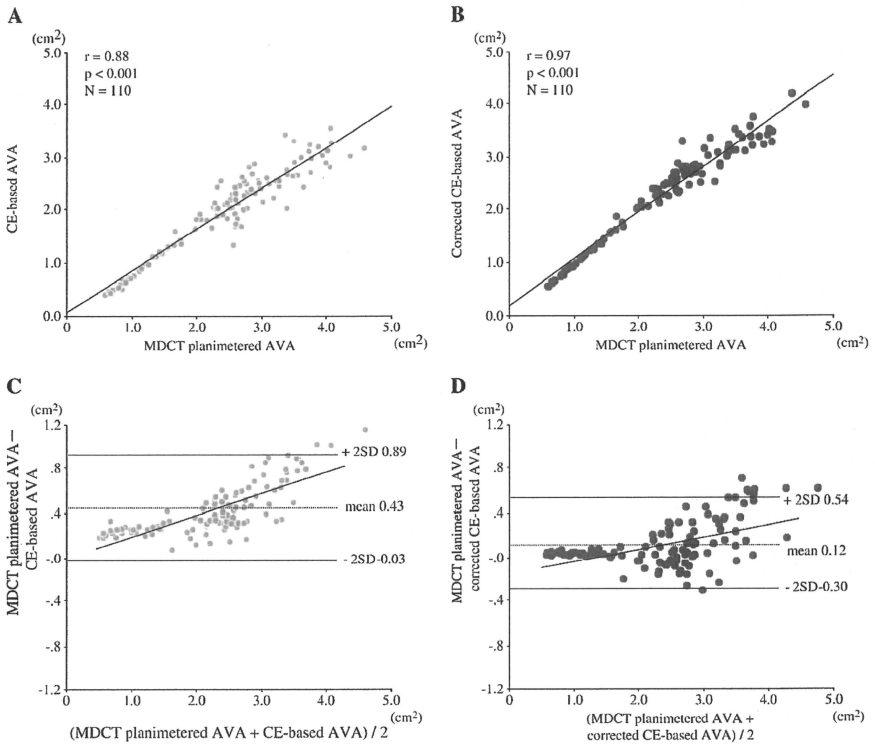
Table 2 shows the correlation between the MDCT planimetered LVOT area and the ellipticity index with the patients' demographic and echocardiographic variables. The LVOT area was the parameter most highly correlated with height (r=0.63; p<0.001), followed by the BSA (r=0.57; p<0.001). These correlations remained robust after adjustment for age. After indexing for BSA, the LVOT area was found to be similar in both genders (277 $\pm$ 45 mm^2/m^2 in men versus 275 $\pm$ 30 mm^2/m^2 in women; p=0.43). In addition, the ellipticity index did not differ significantly between both genders (0.20 $\pm$ 0.05 in men versus 0.21 $\pm$ 0.04 in women; p=0.40).

3.2. Planimetered LVOT area and ellipticity in patients with calcified aortic valve disease

The mean difference between the short- and long-axis LVOT diameters was 5.5 $\pm$ 1.6 mm, and the ellipticity index was 0.20 $\pm$ 0.04. The Pearson correlation coefficient between LVOT diameter

values measured using echocardiography and MDCT was 0.78 (p<0.001). The LVOT diameter measured using echocardiography (i.e. anteroposterior diameter) corresponded approximately to the short-axis LVOT diameter (mean difference, 0.2 $\pm$ 0.3 mm; p=0.11). This led to the discrepancy in LVOT area measurements between MDCT planimetry and echocardiography. The actual LVOT cross-sectional area was significantly underestimated using echocardiographic diameter-derived LVOT area measurement (444 $\pm$ 70 mm^2 versus 369 $\pm$ 63 mm^2; p<0.001).

The MDCT planimetered LVOT area correlated more closely with the ellipsoidal-estimated LVOT area than with the diameter-derived LVOT area (r=0.98 versus 0.82) (Fig. 2A and B). In addition, Bland–Altman analyses were used to test the agreement between diameter-derived LVOT areas versus MDCT planimetered LVOT areas (Fig. 2C), and ellipsoidal-estimated LVOT areas versus MDCT planimetered LVOT areas (Fig. 2D). The ellipsoidal-estimated LVOT area had narrower limits of agreement and less bias. The mean differences between the MDCT planimetered LVOT area and the diameter-derived LVOT area, and ellipsoidal-estimated LVOT area were 73 $\pm$ 30 mm^2 and -6 ± 12 mm^2, respectively.

Fig. 3. Scatterplot of the correlation between the MDCT planimetered AVA and the continuity equation (CE)-based AVA calculated using echocardiography (A) and that between the MDCT planimetered AVA and the CE-based AVA corrected by using the MDCT planimetered LVOT area in the calculation (B). Bland–Altman plot analysis shows that the MDCT planimetered AVA has a poor agreement with the CE-based AVA (C), whereas has a good agreement with the CE-based AVA corrected using MDCT planimetered LVOT area (D). Bold lines represent regression lines (C; r=0.78, p<0.001, D; r=0.49, p<0.001). Abbreviations are as detailed in Fig. 1.

The mean coefficients of variations, within and across observers, were within an acceptable range for the MDCT planimetered LVOT area (2.7% and 4.4%, respectively) and the ellipticity index (3.1% and 5.3%, respectively).

3.3. Impact of LVOT ellipticity on the AVA measurements

Using CE-based calculations, the AVA was significantly under-estimated relative to the MDCT planimetered AVA (1.99 ± 0.84 cm^2 versus 2.47 ± 1.03 cm^2, p<0.001). When the CE was corrected using the MDCT planimetered LVOT area (i.e. the MDCT planimetered LVOT area was substituted into the CE in place of the diameter-derived LVOT area), the measured values were still significantly smaller than those obtained using planimetry (2.34 ± 0.92 cm^2 versus 2.47 ± 1.03 cm^2, p<0.001), but the difference between both measurements of AVA significantly decreased (p<0.001). The correlation coefficient improved from 0.88 to 0.97 (Fig. 3A and B). Similarly, Bland–Altman analyses revealed that there was better agreement between CE-based AVAs corrected with directly measured LVOT areas and MDCT planimetered AVAs, than between CE-based AVAs and MDCT planimetered AVAs (Fig. 3C and D). The mean differences between the MDCT planimetered AVA and the CE-based AVA, and the corrected CE-based AVA were 0.43 ± 0.23 cm^2 and 0.12 ± 0.21 cm^2, respectively. In patients with severe AS (n=20), 6 patients were reclassified as moderate after CE correction using the MDCT planimetered LVOT area.

Fig. 4A depicts the relationship between the measurement error of CE-based AVA and MDCT planimetered AVA. On average, the MDCT planimetered AVA measurements indicated that the CE-based AVA calculations underestimated values by 18 ± 7%. Notably, patients with severe AS (AVA<1.0 cm^2) had a larger measurement error than others (28 ± 5% versus 16 ± 5%, p<0.001). By correcting the impact of underestimation of LVOT area on the AVA values, the measurement error of CE-based AVA significantly decreased and did not differ between severe AS group and others (5 ± 2% versus 3 ± 6%, p=0.36; Fig. 4B). Percent changes in measurement error were more improved in patients with severe AS than in others (23 ± 3% versus 13 ± 7%, p<0.001).

Fig. 5 shows the echocardiographic and CT findings in a representative case with severe AS. When the CE was corrected by inclusion of the MDCT planimetered LVOT area, the measurement error of the CE-based AVA decreased from 39% to 8%.

4. Discussion

In the present study, we demonstrated the following. 1) The MDCT planimetered LVOT area was positively correlated with body size regardless of gender, whereas the ellipticity index was independent of age, gender and body size. 2) In patients with calcified aortic valves without LVOT obstruction, the anatomy of the LVOT cross-sectional area had an elliptical shape during the midsystolic phase. 3) The diameter-derived LVOT area was smaller than MDCT planimetered LVOT area, resulting in the underestimation of AVA measurements using the CE. 4) The corrected CE-based AVA using the MDCT planimetered LVOT area improved the measurement error of CE-based AVA, especially in patients with severe AS.

4.1. Anatomical observation of LVOT area and geometry assessed by MDCT

Degenerative AS is the most common valvular disease related to an atherosclerotic process [11], valvular inflammation and metabolic disorder [12]. Currently, the American Society of Echocardiography recommends that effective AVA based on the CE be used as the standard method for quantitative evaluation of AS [1]. In the CE, the LVOT area component of the equation is not measured directly but estimated using the LVOT diameter from a parasternal long-axis
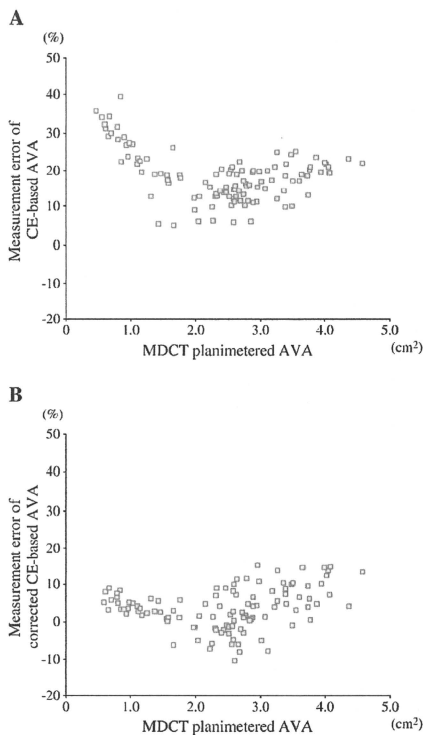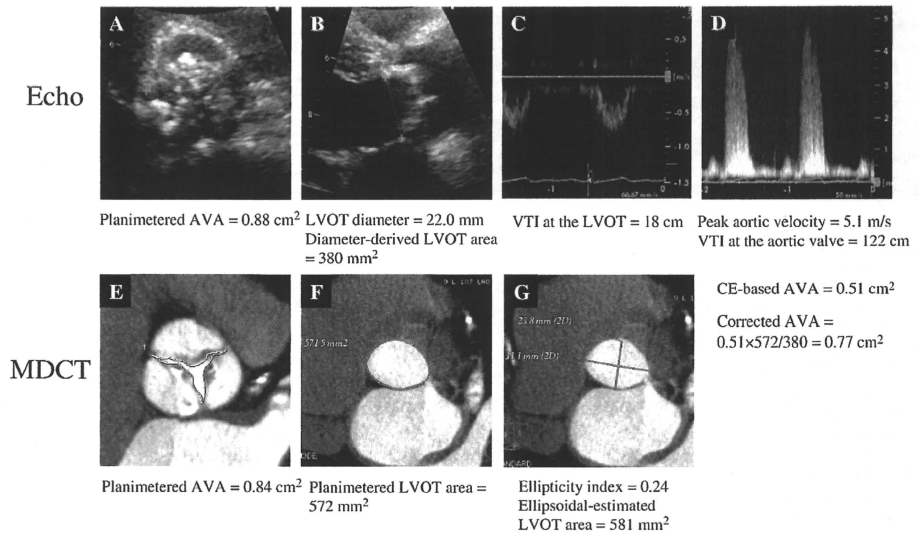
A

B

Fig. 4. Scatterplot of relationship between measurement error of CE-based AVA and MDCT planimetered AVA (A) and that between measurement error of corrected CE-based AVA and MDCT planimetered AVA (B).

view (corresponding to anteroposterior view) assuming a circular geometry. However, in the present study, the MDCT planimetered LVOT area was more closely related to the ellipsoidal-estimated LVOT area than the diameter-derived LVOT area, indicating that the cross section of the LVOT is oval during the midsystolic phase. Furthermore, echocardiographically derived anteroposterior measurements of LVOT diameters correspond approximately to the minor diameters of an elliptical LVOT, resulting in significant underestimations of the actual cross-sectional LVOT areas. These findings are in agreement with those detailed in the most recent report where 64-MDCT was used, but the study population was limited to patients with severe AS referred for transcatheter aortic valve implantations (TAVI) [13].

4.2. LVOT ellipticity and CE-based measurements of AVA

Our results showed that CE-based AVA generally underestimated MDCT planimetered AVA, with a mean measurement error of 18%. Gilon et al. reported that the discrepancy between both measurements of AVA ranged from 10% to 30% and varied prominently with valve shape [14]. Other explanations about the observed discrepancy

Echo

Planimetered AVA = 0.88 cm^2 (A)   LVOT diameter = 22.0 mm   VTI at the LVOT = 18 cm   Peak aortic velocity = 5.1 m/s
Diameter-derived LVOT area   VTI at the aortic valve = 122 cm
= 380 mm^2

MDCT

                                                            CE-based AVA = 0.51 cm^2

                                                            Corrected AVA =
                                                            0.51×572/380 = 0.77 cm^2

Planimetered AVA = 0.84 cm^2 (E)   Planimetered LVOT area =   Ellipticity index = 0.24
                                       572 mm^2 Ellipsoidal-estimated
                                                            LVOT area = 581 mm^2

Fig. 5. The echocardiographic planimetered AVA is 0.88 cm^2 (A). The echocardiographic LVOT diameter is 22.0 mm and the diameter-derived LVOT area is calculated as 380 mm^2 (B). Doppler tracings show the velocity–time integral (VTI) at the LVOT (C) and the aortic valve (D). The CE-based AVA is calculated as 0.51 cm^2. Meanwhile, the MDCT planimetered AVA is 0.84 cm^2 (E). From a double oblique transversal image of the LVOT, the LVOT area is directly measured as 572 mm^2 (F) and the ellipsoidal-estimated LVOT area is calculated as 581 mm^2 (G). When the CE is corrected with the MDCT planimetered LVOT area, the CE-based AVA is corrected to 0.77 cm^2. The measurement error decreases from 39% to 8%. Abbreviations are as detailed in Fig. 1.

between CE-based AVA and planimetered AVA have been put forward. This discrepancy may represent the difference between the anatomic AVA (geometric orifice area) measured with planimetry and the averaged effective AVA (effective orifice area) computed using the CE [2]. The planimetered AVA indicates the maximal opening area in the systolic phase, whereas the CE-based AVA indicates the average systolic opening of the aortic valve because the VTI is a time-averaged systolic velocity [8]. If the ascending aorta is narrow, pressure recovery phenomenon distal to the stenosis can lead to a measurement error in the CE-based AVA [15,16].

In the present study, the actual cross-sectional LVOT area was underestimated using diameter-derived LVOT area calculations due to the assumption of circular geometry. Notably, the ellipticity index was larger in severe AS patients than in others, resulting in larger measurement error of CE-based AVA ranging from 20 to 39%. When the MDCT planimetered LVOT area was included in the CE, measurement error significantly decreased in patients with severe AS more than in others. Thus, we suggest that the difference in LVOT area calculations due to the assumption of a circular or ellipsoidal geometry is one of the major causes of the discrepancy between CE-based AVA and planimetered AVA values. This finding reveals CE's weak points for assessment of AS, but has only been validated in a small number of AS patients in the previous study [6]. The present study has now clearly demonstrated the impact of LVOT ellipticity on the measurement error associated with the CE-based AVA in this setting. The application of cardiac MDCT would contribute to an advance in echocardiographic diagnosis and clinical decision making, particularly in patients with severe AS, as it frequently performs due to the necessity for pre-implantation measurements prior to TAVI.

4.3. Factors related to LVOT area and ellipticity

In the present study, the MDCT planimetered LVOT area was positively correlated with BSA and height regardless of gender. Leye et al. have shown that the LVOT diameter has a good correlation with both BSA and height, independent of gender in adult AS patients [10]. However, few data are available on the relationship between actual LVOT cross-sectional area and various morphometric parameters, such as BSA and height.

Interestingly, the ellipticity index was positively correlated with peak aortic valve velocity, LV wall thickness and LV mass index, independent of age, gender and body size. A recent study has shown that LVOT geometry is more elliptical in patients with severe AS before TAVI, with a mean ellipticity index of 0.26 [13]. After AS treatment with TAVI, LVOT geometry changed to being more circular. In view of our findings, this change may result from LV reverse remodeling with regression of LV mass.

4.4. Study limitations

Firstly, there is no true gold standard for AVA calculation in this study. However, cardiac MDCT has a superior spatial signal-to-noise ratio, as compared with echocardiography, and thus would provide more detailed information about cardiac shape, effectively acting as a "clinical gold standard". Secondly, because exposure to radiation is still high during cardiac MDCT examination [17], we do not recommend this modality as a first choice for the evaluation of AS, either initially or for serial follow-up. Echocardiography including 3D volumetric imaging remains the first choice for the assessment of AS severity. Thirdly, the limits of temporal resolution with 64-MDCT would result in inadequate visualization of the valve leaflet and the

LVOT in patients with rapid or irregular heart rhythms. However, in our study, we did not need to exclude any patient because of inadequate image quality.

Finally, patients with bicuspid aortic valves, sigmoid septum, and ejection fraction <50% were excluded from this study because of the confounding effect in the assessment of the severity of AS [18,19]. Furthermore, the "dimensions" of Japanese patients in this study were relatively small. Thus, larger observational studies including other ethnic group are necessary to confirm our findings.

5. Conclusions

In patients with calcified aortic valve disease including AS, CE-based calculations have generally underestimated AVA values as compared with the corresponding values obtained using MDCT planimetered AVA measurements. This discrepancy is considered to be related to the fact that LVOT geometry is actually elliptical rather than circular.

Acknowledgment

References

[1] Baumgartner H, Hung J, Bermejo J, et al. Echocardiographic assessment of valve stenosis: EAE/ASE recommendations for clinical practice. J Am Soc Echocardiogr 2009;22:1–23.

[2] Pouleur AC, le Polain de Waroux JB, Pasquet A, Vancraeynest D, Vanoverschelde JL, Gerber BL. Planimetric and continuity equation assessment of aortic valve area: head to head comparison between cardiac magnetic resonance and echocardiography. J Magn Reson Imaging 2007;26:1436–43.

[3] Feuchtner GM, Dichtl W, Friedrich GJ, et al. Multislice computed tomography for detection of patients with aortic valve stenosis and quantification of severity. J Am Coll Cardiol 2006;47:1410–7.

[4] Tops LF, Wood DA, Delgado V, et al. Noninvasive evaluation of the aortic root with multislice computed tomography implications for transcatheter aortic valve replacement. JACC Cardiovasc Imaging 2008;1:321–30.

[5] Doddamani S, Grushko MJ, Makaryus AN, et al. Demonstration of left ventricular outflow tract eccentricity by 64-slice multi-detector CT. Int J Cardiovasc Imaging 2009;25:175–81.

[6] Halpern EJ, Mallya R, Sewell M, Shulman M, Zwas DR. Differences in aortic valve area measured with CT planimetry and echocardiography (continuity equation) are related to divergent estimates of left ventricular outflow tract area. AJR Am J Roentgenol 2009;192:1668–73.

[7] Abbara S, Pena AJ, Maurovich-Horvat P, et al. Feasibility and optimization of aortic valve planimetry with MDCT. AJR Am J Roentgenol 2007;188:356–60.

[8] Lang RM, Bierig M, Devereux RB, et al. Recommendations for chamber quantification: a report from the American Society of Echocardiography's Guidelines and Standards Committee and the Chamber Quantification Writing Group, developed in conjunction with the European Association of Echocardiography, a branch of the European Society of Cardiology. J Am Soc Echocardiogr 2005;18:1440–63.

[9] Schiller NB, Shah PM, Crawford M, et al. Recommendations for quantitation of the left ventricle by two-dimensional echocardiography. American Society of Echocardiography Committee on Standards, Subcommittee on Quantitation of Two-Dimensional Echocardiograms. J Am Soc Echocardiogr 1989;2:358–67.

[10] Leye M, Brochet E, Lepage L, et al. Size-adjusted left ventricular outflow tract diameter reference values: a safeguard for the evaluation of the severity of aortic stenosis. J Am Soc Echocardiogr 2009;22:445–51.

[11] Corciu AI, Siciliano V, Poggianti E, Petersen C, Venneri L, Picano E. Cardiac calcification by transthoracic echocardiography in patients with known or suspected coronary artery disease. Int J Cardiol 2010;142:288–95.

[12] Mohty D, Pibarot P, Despres JP, et al. Age-related differences in the pathogenesis of calcific aortic stenosis: the potential role of resistin. Int J Cardiol 2010;142:126–32.

[13] Ng ACT, Delgado V, van der Kley F, et al. Comparison of aortic root dimensions and geometries before and after transcatheter aortic valve implantation by 2- and 3-dimensional transesophageal echocardiography and multislice computed tomography. Circ Cardiovasc Imaging 2010;3:94–102.

[14] Gilon D, Cape EG, Handschumacher MD, et al. Effect of three-dimensional valve shape on the hemodynamics of aortic stenosis: three-dimensional echocardiographic stereolithography and patient studies. J Am Coll Cardiol 2002;40:1479–86.

[15] Richardson-Lobbedez M, Ennezat PV, Marechaux S. Critical impact of pressure recovery on assessment of aortic valve stenosis. Arch Cardiovasc Dis 2009;102:669–70.

[16] Baumgartner H, Stefenelli T, Niederberger J, Schima H, Maurer G. "Overestimation" of catheter gradients by Doppler ultrasound in patients with aortic stenosis: a predictable manifestation of pressure recovery. J Am Coll Cardiol 1999;33:1655–61.

[17] Pontone G, Andreini D, Bartorelli AL, et al. Diagnostic accuracy of coronary computed tomography angiography: a comparison between prospective and retrospective electrocardiogram triggering. J Am Coll Cardiol 2009;54:346–55.

[18] Poh KK, Levine RA, Solis J, et al. Assessing aortic valve area in aortic stenosis by continuity equation: a novel approach using real-time three-dimensional echocardiography. Eur Heart J 2008;29:2526–35.

[19] Donal E, Novaro GM, Deserrano D, et al. Planimetric assessment of anatomic valve area overestimates effective orifice area in bicuspid aortic stenosis. J Am Soc Echocardiogr 2005;18:1392–8.

[20] Shewan LG, Coats AJ. Ethics in the authorship and publishing of scientific articles. Int J Cardiol 2010;144:1–2.

Association Between Visceral Adipose Tissue Area and Coronary Plaque Morphology Assessed by CT Angiography

Norihiko Ohashi, MD,* Hideya Yamamoto, MD, PhD,* Jun Horiguchi, MD, PhD,†
Toshiro Kitagawa, MD, PhD,* Eiji Kunita, MD,* Hiroto Utsunomiya, MD,*
Toshiharu Oka, MD,* Nobuoki Kohno, MD, PhD,‡ Yasuki Kihara, MD, PhD*

Hiroshima, Japan

OBJECTIVES We sought to investigate the association between visceral adipose tissue (VAT) with the presence, extent, and characteristics of noncalcified coronary plaques (NCPs) using 64-slice computed tomography angiography (CTA).

BACKGROUND Although visceral adiposity is associated with cardiovascular events, its association with NCP burden and vulnerability is not well known.

METHODS The study population consisted of 427 patients (age 67 ± 11 years; 63% men) with proven or suspected coronary artery disease who underwent 64-slice CTA. We assessed the presence and number of NCPs for each patient. The extent of NCP was tested for the difference between high (≥2) and low (≤1) counts. We further evaluated the vulnerable characteristics of NCPs with positive remodeling (remodeling index >1.05), low CT density (≤38 HU), and the presence of adjacent spotty calcium. Plain abdominal scans were also performed to measure the VAT and subcutaneous adipose tissue area.

RESULTS A total of 260 (61%) patients had identifiable NCPs. Multivariate analyses revealed that increased VAT area (per 1 standard deviation, 58 cm²) was significantly associated with both the presence (odds ratio [OR]: 1.68; 95% confidence interval [CI]: 1.28 to 2.22) and extent (OR: 1.31; 95% CI: 1.03 to 1.68) of NCP. Other body composition measures, including subcutaneous adipose tissue area, body mass index, and waist circumference, were not significantly associated with either presence or extent of NCP. Increased VAT area was also independently associated with the presence of NCP with positive remodeling (OR: 1.71; 95% CI: 1.18 to 2.53), low CT density (OR: 1.69; 95% CI: 1.17 to 2.47), and adjacent spotty calcium (OR: 1.52; 95% CI: 1.03 to 2.27).

CONCLUSIONS Increased VAT area was significantly associated with NCP burden and vulnerable characteristics identified by CTA. Our findings may explain the excessive cardiovascular risk in patients with visceral adiposity, and support the potential role of CTA to improve risk stratification in such patients. (J Am Coll Cardiol Img 2010;3:908–17) © 2010 by the American College of Cardiology Foundation

Obesity is widely accepted as a risk factor for coronary artery disease (CAD) (1). In particular, visceral adipose tissue (VAT) accumulation was reported to be a better predictor of metabolic abnormalities and atherosclerosis than total body fat (2,3). Recent epidemiological studies have also suggested that visceral adiposity, as evaluated by the waist-to-hip ratio (4) or computed tomography (CT) scanning (5), is more closely related to cardiovascular events than is body mass index (BMI), a crude marker of total adiposity.

See page 918

We previously reported that VAT area is associated with the presence and extent of coronary artery calcium (CAC), independently of BMI, using multidetector CT (6). Whereas the presence and extent of CAC are strongly associated with the overall atherosclerotic plaque burden, it is assumed that noncalcified coronary plaques (NCPs), which contain lipid-rich components and display positive remodeling (PR), are more prone to rupture with subsequent coronary events, according to results of intravascular ultrasound (IVUS) (7) and pathologic (8) studies.

Recent advances in cardiac CT angiography (CTA) have enabled noninvasive detection of NCPs (9–12). Moreover, we previously reported that 64-slice CTA can be used to characterize NCPs in terms of composition (e.g., predominantly fibrous vs. lipid-rich plaques), vascular remodeling, and adjacent calcium morphology. We also reported that 64-slice CTA shows good agreement with IVUS (11).

To our knowledge, very few studies have examined the association between VAT, as an entity, with NCP, particularly regarding its composition and morphology. Determining the associations between VAT area and NCP burden or vulnerable characteristics seems to be important from an etiological perspective. Therefore, in this study, we used 64-slice CTA to quantitatively and qualitatively assess coronary artery plaques to determine whether VAT area is associated with the presence, extent, and vulnerable characteristics of NCPs.

METHODS

Study patients. Between November 2006 and December 2008, we recruited 565 consecutive Japanese patients with proven or suspected CAD, who underwent 64-slice CTA for the follow-up or diagnosis of CAD at our institution. For the present study, we excluded 138 subjects with a history of percutaneous coronary intervention (n = 63) or coronary artery bypass grafting (n = 62), subjects with poor image quality because of motion artifacts or inadequate contrast concentration (n = 6), and subjects with missing information for 1 or more traditional CAD risk factors (n = 7). As a result, 427 patients (267 men and 160 women, 67 ± 11 years) were finally enrolled and included in this study. In all patients, plain cardiac and abdominal scans were performed to measure the CAC score and the VAT area. The study was approved by the hospital's ethical committee, and written informed consent was obtained from all patients.

Risk factor assessment. All patients provided details of their demographics, medical history, and medications at the clinical consultation. Patients were considered current smokers if they had smoked at least 1 cigarette a day within the previous year. Hypertension was defined as systolic blood pressure ≥ 140 mm Hg, diastolic blood pressure ≥ 90 mm Hg, or on antihypertensive therapy. Diabetes mellitus was defined by self-report, a hemoglobin A_{1c} level $\geq 6.5\%$ (13), or current use of hypoglycemic agents. Hypercholesterolemia was characterized by a fasting serum low-density lipoprotein cholesterol level ≥ 140 mg/dl on direct measurement (14) or current use of lipid-lowering agents. Height (m) and body weight (kg) were used to calculate BMI.

Coronary CT scan protocol and reconstruction. CT examinations were performed using a 64-slice CT scanner (LightSpeed VCT, GE Healthcare, Waukesha, Wisconsin) with a gantry rotation time of 350 ms. To avoid motion artifacts, patients with a resting heart rate ≥ 60 beats/min were orally administered 40 mg of metoprolol at 60 min before the CT scan. All patients received 0.3 mg of nitroglycerin sublingually just before scanning. A noncontrast-enhanced scan with prospective electrocardiographic gating was performed before CTA to measure the CAC score (sequential scan with 16 $\times$ 2.5-mm collimation; tube current, 140 mA; tube voltage, 120 kV). Following a test bolus examination to determine the start of the contrast-enhanced scan, a retrospective electrocardiogram-gated CTA was performed using a helical mode during an

inspiratory breath-hold (64 × 0.625-mm collimation; CT pitch factor, 0.18 to 0.24:1; tube current, 600 to 750 mA with electrocardiogram-correlated tube current modulation; tube voltage, 120 kV). A body weight–adjusted volume (0.6 to 0.7 ml/kg) of contrast material (iopamidol, 370 mg I/ml, Bayer Healthcare, Berlin, Germany) was injected over the course of 10 s, followed by a saline flush of 25 ml. The effective radiation dose was estimated based on the dose-length product and ranged from 15 to 18 mSv (11).

Image reconstruction was retrospectively gated to the electrocardiogram. Depending on the heart rate, either a half-scan (temporal window = 175 ms) or a multisegment (temporal window <175 ms) reconstruction algorithm was selected, and the optimal cardiac phase with the fewest motion artifacts was chosen individually. The reconstructed image data were transferred to a remote computer workstation for post-processing (Advantage Workstation Ver.4.2, GE Healthcare) and were analyzed using dedicated software (CardIQ, GE Healthcare).

CAC scoring. CAC score was assessed by 2 blinded and independent observers using semiautomatic software (Smartscore, version 3.5, GE Healthcare). In each patient, CAC was identified as a dense area in the coronary artery exceeding the threshold of 130 HU, and the total CAC score was calculated based on the Agatston method (15).

Evaluation of plaque characteristics. All coronary segments >2 mm in diameter were evaluated by 2 blinded and independent observers using curved multiplanar reconstructions and cross-sectional images rendered perpendicular to the vessel center line. Atherosclerotic plaques were classified as calcified or noncalcified. Calcified plaques were defined as lesions composed exclusively of structures with a CT density greater than that of the contrast-enhanced coronary lumen, or with a CT density of >130 HU assigned to the coronary artery wall in a plain image. NCPs were defined as a low-density mass >1 mm² in size, located within the vessel wall, and clearly distinguishable from the contrast-enhanced coronary lumen and the surrounding pericardial tissue. For the analysis of plaque characteristics, the optimal image display setting was chosen on an individual basis; in general, the window was between 700 and 1,000 HU, and the level was between 100 and 200 HU.

We further evaluated the NCP characteristics on CTA by determining the minimum CT density, the vascular remodeling index, and adjacent calcium

morphology, as previously described (11). The minimum CT density was determined as the lowest density of at least 5 regions of interest (area = 1 mm²), which were placed on each lesion in a random order. Based on our previous comparison of CTA and IVUS data (11), NCP ≤38 HU (corresponding to IVUS-identified hypoechoic plaque) was defined as a low-density plaque. We then measured the cross-sectional vessel area (mm²) for each NCP site by manually tracing the outer vessel contour (border to low-signal epicardial fat). Vascular remodeling was assessed using the remodeling index, which was calculated by dividing the cross-sectional lesion vessel area by the proximal reference vessel area. PR was defined as remodeling index >1.05 (12). Finally, based on the methods previously described (11,16), we classified calcium deposits in or adjacent to each NCP morphologically according to their length (L) and width (W) versus the vessel diameter (VD) of the coronary artery in which the calcium was observed as follows: none, undetectable; spotty, L < 3/2 of VD and W < 2/3 of VD; long, L ≥ 3/2 of VD and W < 2/3 of VD; wide, L < 3/2 of VD and W ≥ 2/3 of VD; and diffuse, L ≥ 3/2 of VD and W ≥ 2/3 of VD.

Measurement of VAT area. In addition to cardiac scans, abdominal scans were performed at the 4th to 5th lumbar levels in the spinal position, and 12 slices at 5-mm thickness were obtained during a breath-hold after normal expiration. The adipose tissue areas and waist circumference in each subject were determined from an image taken at the level of the umbilicus using dedicated software (Virtual Place, AZE Inc., Tokyo, Japan). Subcutaneous adipose tissue was defined as extraperitoneal fat between the skin and muscles, with attenuation ranging from −150 to −50 HU. Intraperitoneal fat with the same density as the subcutaneous adipose tissue layer was defined as VAT. The adipose tissue areas were determined by automatic planimetry. Waist circumference was determined at the umbilicus level using a mobile caliper.

Statistical analysis. Categorical variables are presented as the number of patients (percentage), and continuous variables are expressed as mean ± SD or medians (interquartile range). We compared sex-specific clinical and CTA characteristics between patients divided by the median values of VAT area. Differences between patients with high and low VAT area were evaluated using chi-square tests for categorical variables and the Student *t* test or Mann-Whitney *U* test for continuous variables. The presence of plaque was assessed as a binary